CCD Photometry, Light Curve Modeling, and Period Study of the Overcontact Binary Systems NSVS 7245866 and V685 Pegasi

Kevin B. Alton
UnderOak Observatory, 70 Summit Avenue, Cedar Knolls, NJ; mail@underoakobservatory.com

Received January 1, 2020; revised February 27, 2020; accepted March 2, 2020

Abstract Precise time-series multi-color (B, V, and I_c) light curve data were acquired at UnderOak Observatory (UO) from NSVS 7245866 (2017) and V685 Peg (2016). Prior to this investigation only monochromatic CCD data for both variables were available from automated surveys which employ sparse sampling strategies. Each target produced new times-of-minimum from data acquired at UO as well as values extrapolated from the SuperWASP survey. These results along with other eclipse timings from the literature were used to generate new ephemerides. Roche modeling of the observed light curve data was accomplished using the Wilson-Devinney code. Each system exhibits a total eclipse, therefore a reliable photometrically derived value for the mass ratio (q_{ptm}) was determined which consequently provided initial estimates for the physical and geometric elements of both variable systems.

1. Introduction

Overcontact binaries (OCs), also known as eclipsing W UMa-type (EW) variables, have stellar components that are in varying degrees of physical contact and therefore share a common atmosphere. They represent at least 25% of all eclipsing binaries found in photometric surveys conducted in both Northern and Southern hemispheres (Kepler (Prša *et al.* 2011); ASAS (Paczyński *et al.* 2006); New South Wales Survey (Christiansen *et al.* 2008)). Despite their relatively high abundance, many questions about energy and mass transfer within and between stars remain unanswered. Since OCs have short orbital periods (0.25–1 d) they are attractive targets for photometric study using modestly sized telescopes equipped with CCD cameras. Their corresponding light curves (LCs) typically exhibit eclipse minima of nearly equal depth that show little color change, thereby suggesting that surface temperatures are similar. Radial velocity studies reveal that the majority of OCs have mass ratios ($q = m_2/m_1$) that diverge considerably from unity and have been observed as low as 0.065–0.08 (Sriram *et al.* 2016; Mochnacki and Doughty 1972; Paczyński *et al.* 2007; Arbutina 2009). Overcontact binaries spend most of their evolutionary lifetimes in physical contact (Stępień 2006; Gazeas and Stępień 2008; Stępień and Kiraga 2015). Depending on many factors, including rate of angular momentum loss, mass ratio, total mass, orbital period and metallicity, OCs are destined to merge into fast rotating stars or to alternatively produce exotic objects such as blue stragglers (Qian *et al.* 2006; Stępień and Kiraga 2015), double degenerate binaries, supernovae, or even double black holes (Almeida *et al.* 2015).

Monochromatic CCD-derived photometric data for NSVS 7245866 were first acquired from the ROTSE-I survey between 1999 and 2000 (Akerlof *et al.* 2000; Wozniak *et al.* 2004; Gettel *et al.* 2006). Later on this system was also captured by the Catalina Sky (Drake *et al.* 2014), and SuperWASP (Butters *et al.* 2010) surveys. Similarly, sparsely sampled photometric data for V685 Pegasi (TYC 2258-1489-1) had been acquired from the ROTSE-I, ASAS (Pojmański *et al.* 2005), Catalina, and SuperWASP surveys. The SuperWASP findings for both systems proved to be a rich source of time (HJD) vs. magnitude data and were further examined to extract out new times-of-minimum (ToM) light and generate period-folded light curves. Although other ToM values have been sporadically reported, this paper marks the first detailed period analyses leading to new ephemerides. Data gathered from the Gaia DR2 release of stellar parameters (Andrae *et al.* 2018) and LAMOST DR5 (Zhao *et al.* 2012; Wang *et al.* 2019) improved the reliability of an effective temperature (T_{eff1}) assigned to each primary star. These refined values were subsequently used for Roche modeling of LCs for NSVS 7245866 and V685 Peg using newly acquired multi-color photometric data. As a result, this investigation also provides the first published photometric mass ratio estimates along with preliminary physical and geometric characteristics for each system.

2. Observations and data reduction

Precise time-series photometric data were acquired at UnderOak Observatory (UO; 74.456217 W, 40.825229 N) with a 0.28-m Schmidt-Cassegrain telescope and an ST-8XME CCD camera installed at the Cassegrain focus. Automated imaging was performed with photometric B-, V-, and I_c filters manufactured to match the Johnson-Cousins Bessell prescription. Computer time was updated immediately prior to each session and exposure time for all images adjusted to 60 s (NSVS 7245866) or 75 s (V685 Peg). Details regarding image acquisition (science frames, darks, and flats), calibration, and registration can be found elsewhere (Alton 2016). Only data from images taken above 30° altitude (airmass < 2.0) were used, consequently, error due to differential refraction and color extinction was minimized and not corrected. Instrumental readings were reduced to MPOSC3 catalog-based magnitudes (Warner 2007) built into MPO CANOPUS v10.7.1.3 (Minor Planet Observer 2011).

3. Results and discussion

Further photometric reduction to LCs was accomplished using an ensemble of at least three non-varying comparison stars in the same field of view (FOV). The identities, J2000

coordinates, V-mags, and MPOSC3 color indices (B–V) for these stars are listed in Table 1. CCD images annotated with the location of target and comparison stars are shown for NSVS 7245866 (Figure 1) and V685 Peg (Figure 2). Uncertainty in comparison star measurements made in the same FOV with NSVS 7245866 or V685 Peg typically stayed within ± 0.007 mag for V- and I_c- and ± 0.010 mag for B-passbands. All photometric data from both systems can be downloaded from the AAVSO archives (https://www.aavso.org/data-download).

3.1. Photometry and ephemerides

Times of minimum (ToM) were calculated using the method of Kwee and van Woerden (1956) as implemented in PERANSO v2.6 (Paunzen and Vanmunster 2016). Curve fitting all eclipse timing differences (ETD) was accomplished using scaled Levenberg-Marquardt algorithms (QtiPlot 2013). The results from these analyses are separately discussed for each binary system in the subsections below.

3.1.1. NSVS 7245866

A total of 333 photometric values in B-, 339 in V-, and 337 in I_c-passbands were acquired at UO from NSVS 7245866 between February 18, 2017, and March 6, 2017. Included in these determinations were four new ToM measurements which are summarized in Table 2. The SuperWASP survey (Butters *et al.* 2010) provided a wealth of photometric data taken (30-s exposures) at modest cadence that repeats every 9 to 12 min. Unfiltered data acquired in 2004 and broadband (400–700 nm) measurements made between 2006 and 2008 were offset relative to V-mag data produced at UO (2017) and then folded together (Figure 3; P = 0.406543 d) by applying periodic orthogonals (Schwarzenberg-Czerny 1996) to fit observations and analysis of variance to assess fit quality (PERANSO v2.6). In some cases (n = 41) the SuperWASP data were amenable to further analysis using the method of Kwee and van Woerden (1956) to estimate ToM values. These results (2006–2008), along with other eclipse timings acquired at UO in 2017 (Table 2), were used to calculate a linear ephemeris (Equation 1):

$$\text{Min.I (HJD)} = 2457818.5685\,(8) + 0.4065432\,(1)\,\text{E}. \quad (1)$$

When all ToM data were included (2004–2017), plotting (Figure 4) the difference between the observed eclipse times and those predicted by the linear ephemeris against epoch (cycle number) reveals what appears to be a quadratic relationship (Equation 2) where:

$$\text{ETD} = -1.47 \cdot 10^{-4} + 2.03 \cdot 10^{-6}\text{E} + 2.13 \cdot 10^{-10}\text{E}^2. \quad (2)$$

In this case the ETD residuals vs. epoch can be described by an expression with a positive quadratic coefficient ($+2.13 \cdot 10^{-10}$), suggesting that the orbital period may have been slowly increasing over time at the rate of 0.033 (7) $\text{s} \cdot \text{y}^{-1}$.

It would be remiss, however, not to note that eclipse timing data for NSVS 7245866 are only available since 2004, with a large time gap between 2008 and 2017. Despite the apparent quadratic fit of the ETD residuals illustrated in Figure 4, the best fit simultaneous LC solution (Figure 3) using SuperWASP (2004–2008) and UO (2017) ToM values had very small uncertainty (P = 0.406543 ± 0.000004 d). Arguably, if there is a secular change in the orbital period, the rate would be similar to many other contact systems reported in the literature (Giménez *et al.* 2006). Furthermore, given the paucity of data, it is not surprising that no other underlying variations in the orbital period stand out, such as those that might be caused by magnetic cycles (Applegate 1992) or the presence of an additional gravitationally bound stellar-size body. At a minimum, another decade of precise times of minimum will be needed to reveal whether the orbital period of this system is changing in a predictable fashion.

3.1.2. V685 Peg

A total of 304 photometric values in B-, 303 in V-, and 313 in I_c-passbands were acquired from V685 Peg between October 18, 2016, and November 8, 2016. Included with the ToM data summarized in Table 3 are five new values acquired at UO, 24 times estimated from the SuperWASP survey, as well as three other published times that were used to calculate a new linear ephemeris (Equation 3):

$$\text{Min.I (HJD)} = 2457700.6725\,(4) + 0.3172596\,(4)\,\text{E}. \quad (3)$$

These data, shown in Figure 5, suggest that the orbital period of V685 Peg has not meaningfully changed since 2004. Furthermore, as can be seen (Figure 6), TAMMAG2 values from SuperWASP, which were offset to match the mean V-mag observed in 2016, produced the best fit LC when P = 0.317260 ± 0.000004 d.

3.2. Effective temperature estimation

The primary star is defined as the more massive member of each binary system throughout this paper. The effective temperature of the primary star (T_{eff1}) was derived from a composite of astrometric (USNO-A2.0, USNO-B1.0, and UCAC4) and photometric (2MASS, SDSS-DR8, and APASS) survey measurements (B–V), low resolution spectra obtained from LAMOST-DR5 (Zhao *et al.* 2012; Wang *et al.* 2019), the Gaia DR2 release of stellar parameters (Andrae *et al.* 2018), and color index (B–V) data acquired at UO. Interstellar extinction (A_V) was calculated using the reddening value (E(B–V)) estimated from the median of six Galactic dust map models (Amôres *et al.* 2011) reproduced within the GALExtin VO-service (http://www.galextin.org/v1p0/).

Intrinsic color, $(B–V)_0$, for NSVS 7245866 calculated from measurements made at UO and those determined from five other sources are listed in Table 4. The median value (0.505 ± 0.093) indicates a primary star with an effective temperature (6260 ± 333 K) that probably ranges in spectral class between F6V and F7V. Houdashelt *et al.* (2000) reported an improved color-temperature relation for cool dwarf stars ($0.32 \leq (B–V) \leq 1.35$) wherein T_{eff1} was calculated to be 6204 ± 380 K. These results, when combined with other T_{eff1} estimates from Gaia DR2 (6066^{+202}_{-140} K) and LAMOST DR5 (6254 ± 14), produced a median value of 6230 ± 267 K which was used for subsequent Roche modeling. Notably, this determination is consistent with the spectral type assigned (F5V) to NSVS 7245866 based on

Table 1. Astrometric coordinates (J2000), V-mags and color indices (B–V) for NSVS 7245866 (Figure 1), V685Peg (Figure 2), and their corresponding comparison stars used in this photometric study.

Star Identification	*R. A. (J2000)* *h m s*	*Dec. (J2000)* *° ′ ″*	*V-mag*[a]	*(B-V)*[a]
(T) NSVS 7245866	07 36 53.06	+34 40 20.60	11.253	0.443
(1) GSC 02461-02062	07 36 57.76	+34 41 58.03	11.230	0.478
(2) GSC 02461-02214	07 36 43.07	+34 39 32.47	12.271	0.482
(3) GSC 02461-01637	07 36 23.34	+34 36 56.22	10.379	0.258
(4) GSC 02461-01381	07 36 41.69	+34 42 37.69	11.999	0.442
(5) GSC 02461-01073	07 37 01.50	+34 44 48.88	12.188	0.569
(T) V685 Peg	23 53 19.50	+28 23 49.68	11.707	0.685
(1) GSC 02258-01111	23 53 59.13	+28 26 57.01	10.116	0.653
(2) GSC 02258-01840	23 53 01.00	+28 18 39.27	11.690	0.738
(3) GSC 02258-01581	23 53 41.07	+28 19 21.59	11.977	1.005

[a]*V-mag and (B–V) for comparison stars derived from MPOSC3 database described by Warner (2007).*

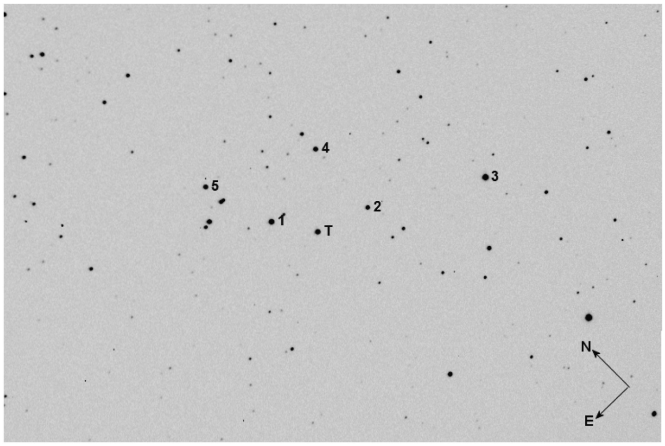

Figure 1. CCD image (V-mag) of NSVS 7245866 (T) showing the location of comparison stars (1–5) used to generate MPOSC3-derived magnitude estimates.

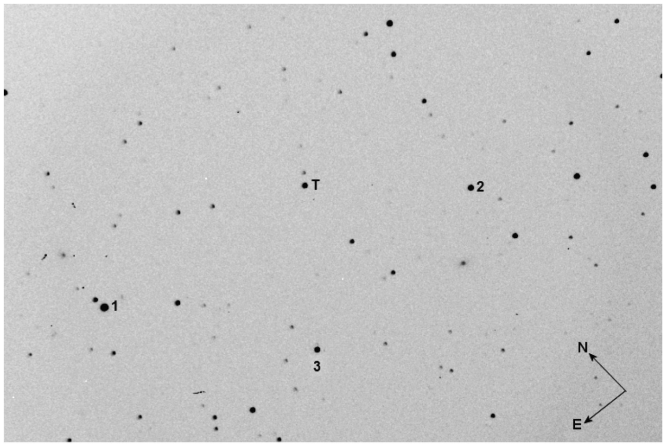

Figure 2. CCD image (V-mag) of V685 Peg (T) showing the location of comparison stars (1–3) used to generate MPOSC3-derived magnitude estimates.

low-resolution spectra taken in 2017 and reported in LAMOST DR5 (http://dr5.lamost.org/spectrum/view?obsid=535813088).

Similarly, dereddened color indices from UO and five other sources are summarized for V685 Peg in Table 5. The median value (0.718 ± 0.047) corresponds to a primary star with an effective temperature (5520 ± 186 K) that likely ranges in spectral class between G7V and G8V. As above, this result, when combined with the value (T_{eff1} = 5521 ± 270 K) calculated according to Houdashelt *et al.* (2000), the Gaia DR2 estimate (5355^{+149}_{-92} K), and that reported (5582 ± 23 K) in LAMOST DR5, yielded a median of 5521 ± 168 K which was adopted for ensuant Roche modeling. Based on a low resolution spectrum (http://dr5.lamost.org/spectrum/view?obsid=490308235) reported in LAMOST DR5, the spectral classification of the primary star is G7V, a result consistent with the V685 Peg color-temperature data presented herein.

Table 2. NSVS 7245866 times-of-minimum (September 29, 2004–March 6, 2017), cycle number and residuals (ETD) between observed and predicted times derived from the updated linear ephemeris (Equation 1).

HJD (2400000 +)	*HJD Error*	*Cycle Number*	*Eclipse Time Difference*	*Reference*
53277.68797	0.0005	–11169.5	0.00349	1
53278.70647	0.0007	–11167	0.00564	1
54056.62331	0.0007	–9253.5	0.00206	1
54057.63575	0.0009	–9251	–0.00186	1
54067.59702	0.0003	–9226.5	–0.00090	1
54070.64627	0.0003	–9219	–0.00072	1
54083.65866	0.0006	–9187	0.00229	1
54084.67078	0.0004	–9184.5	–0.00196	1
54085.68981	0.0002	–9182	0.00072	1
54092.6018	0.0008	–9165	0.00148	1
54098.70019	0.0005	–9150	0.00171	1
54099.51119	0.0003	–9148	–0.00037	1
54099.71531	0.0005	–9147.5	0.00048	1
54100.52696	0.0004	–9145.5	–0.00096	1
54101.54608	0.0004	–9143	0.00181	1
54111.50419	0.0002	–9118.5	–0.00040	1
54115.57181	0.0006	–9108.5	0.00180	1
54118.61771	0.0007	–9101	–0.00138	1
54120.65221	0.0003	–9096	0.00040	1
54122.47948	0.0004	–9091.5	–0.00177	1
54135.48954	0.0006	–9059.5	–0.00109	1
54139.55809	0.0007	–9049.5	0.00202	1
54140.57325	0.0008	–9047	0.00083	1
54141.38471	0.0004	–9045	–0.00080	1
54141.58998	0.0010	–9044.5	0.00120	1
54142.40159	0.0005	–9042.5	–0.00028	1
54142.60458	0.0009	–9042	–0.00056	1
54145.45119	0.0003	–9035	0.00025	1
54146.4653	0.0009	–9032.5	–0.00200	1
54150.53261	0.0005	–9022.5	–0.00012	1
54153.37728	0.0005	–9015.5	–0.00125	1
54153.58513	0.0005	–9015	0.00333	1
54154.39456	0.0005	–9013	–0.00033	1
54155.40972	0.0004	–9010.5	–0.00153	1
54156.42874	0.0005	–9008	0.00113	1
54162.52576	0.0003	–8993	0.00001	1
54163.53846	0.0007	–8990.5	–0.00366	1
54168.41671	0.0009	–8978.5	–0.00392	1
54170.45072	0.0009	–8973.5	–0.00263	1
54171.46803	0.0007	–8971	–0.00167	1
54539.38955	0.0001	–8066	–0.00176	1
57804.54332	0.0001	–34.5	0.00028	2
57805.55905	0.0001	–32	–0.00035	2
57815.51906	0.0001	–7.5	–0.00065	2
57818.56878	0.0001	0	0.00000	2

References: 1. SuperWASP (Butters et al. *2010); 2. This study at UO.*

3.3. Roche modeling approach

Roche modeling of LC data from NSVS 7245866 and V685 Peg was performed with PHOEBE 0.31a (Prša and Zwitter

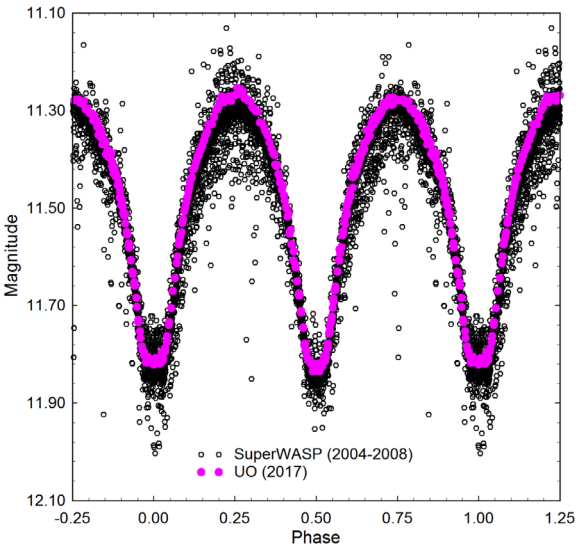

Figure 3. Period folded (P = 0.406543 ± 0.000004 d) light curve data (TAMMAG2 vs. HJD) for NSVS 7245866 acquired from the SuperWASP Survey (2004–2008) and V-mag measurements made at UO in 2017.

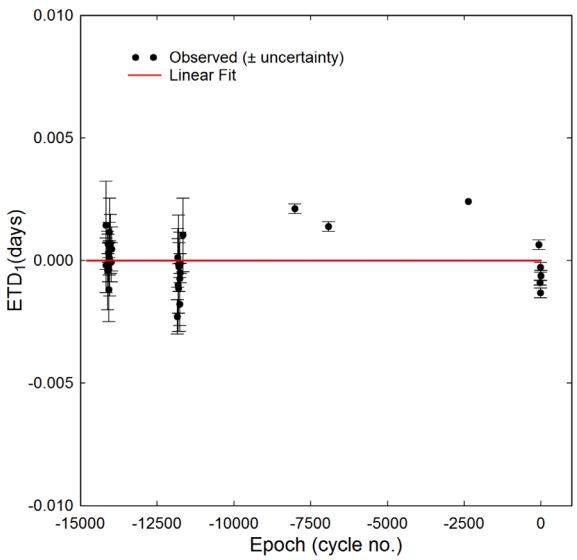

Figure 5. Eclipse timing differences (ETD) vs. epoch for V685 Peg calculated using the updated linear (Equation 3). Measurement uncertainty is denoted by the hatched vertical lines. The solid red line within the figure indicates the Levenberg-Marquardt derived linear fit.

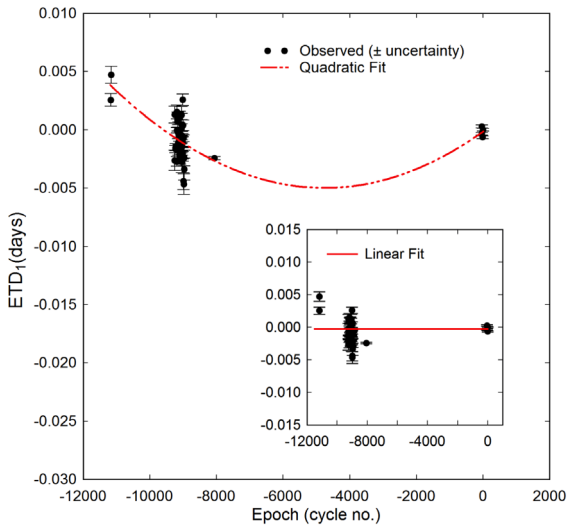

Figure 4. Eclipse timing differences (ETD) vs. epoch for NSVS 7245866 calculated using the updated linear (Equation 1) and quadratic ephemerides (Equation 2). Measurement uncertainty is denoted by the hatched vertical lines. The dashed red line represents the quadratic fit while the solid red line within the figure insert indicates the linear fit.

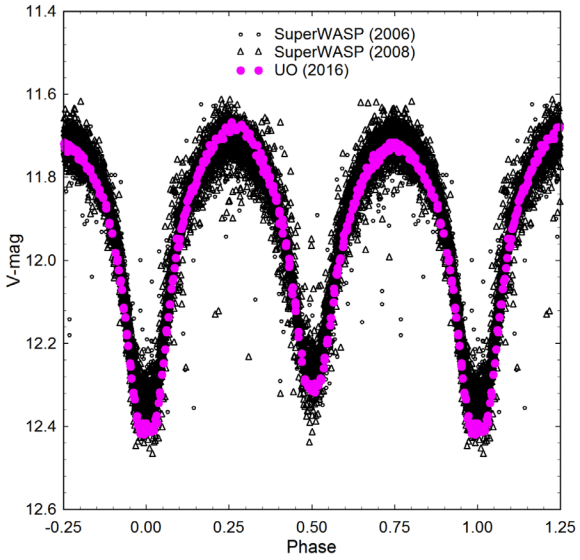

Figure 6. Period folded (P = 0.317260 ± 0.000004 d) light curve data (TAMMAG2 vs. HJD) for V685 Peg acquired from the SuperWASP Survey in 2006 and 2008 and V-mag measurements made at UO in 2016.

2005) and WDWINT56A (Nelson 2009). Both programs feature a MSWINDOWS-compatible GUI interface to the Wilson-Devinney WD 2003 code (Wilson and Devinney 1971; Wilson 1979; Wilson 1990). WDWINT56A incorporates Kurucz's atmosphere models (Kurucz 2002) that are integrated over BVR$_c$I$_c$ passbands. In both cases, the selected model was Mode 3 for an overcontact binary. Other modes (detached and semi-detached) were explored but never approached the goodness of fit achieved with Mode 3. Since the internal energy transfer to the surface of both variable systems is driven by convective (< 7500 K) rather than radiative processes, the value for bolometric albedo ($A_{1,2}$ = 0.5) was assigned according to Ruciński (1969) while the gravity darkening coefficient ($g_{1,2}$ = 0.32) was adopted from Lucy (1967). Logarithmic limb darkening coefficients (x_1, x_2, y_1, y_2) were interpolated (Van Hamme 1993) following each change in the effective temperature (T_{eff2}) of the secondary star during model fit optimization using differential corrections (DC). All but the temperature of the more massive star T_{eff1}, $A_{1,2}$, and $g_{1,2}$ were allowed to vary during DC iterations. In general, the best fits for T_{eff2}, i, q, and Roche potentials ($\Omega_1 = \Omega_2$) were collectively refined (method of multiple subsets) by DC using the multicolor LC data until a simultaneous solution was found. LCs from NSVS 7245866 (Figures 7 and 8) and V685 Peg (Figures 9 and 10) exhibit asymmetry during quadrature (Max I ≠ Max II) which is often called the O'Connell effect (O'Connell 1951). Both systems required the addition of spots to obtain the

Table 3. V685 Peg times-of-minimum (July 17, 2004–November 8, 2016), cycle number and residuals (ETD) between observed and predicted times derived from the updated linear ephemeris (Equation 3).

HJD (2400000 +)	HJD Error	Cycle Number	Eclipse Time Difference	Reference
53203.6776	0.0018	–14174.5	0.00144	1
53207.6417	0.0011	–14162	–0.00020	1
53220.6492	0.0016	–14121	–0.00042	1
53228.5817	0.0004	–14096	0.00068	1
53229.5328	0.0008	–14093	–0.00007	1
53232.5471	0.0004	–14083.5	0.00031	1
53235.5596	0.0013	–14074	–0.00119	1
53238.5748	0.0007	–14064.5	0.00011	1
53239.5277	0.0004	–14061.5	0.00115	1
53242.5410	0.0020	–14052	0.00054	1
53253.4866	0.0012	–14017.5	0.00068	1
53259.5138	0.0008	–13998.5	–0.00007	1
53263.6387	0.0009	–13985.5	0.00047	1
53944.6337	0.0007	–11839	–0.00230	1
53947.6501	0.0012	–11829.5	0.00011	1
53952.5665	0.0019	–11814	–0.00101	1
53953.6768	0.0010	–11810.5	–0.00114	1
53954.6295	0.0020	–11807.5	–0.00016	1
53961.6091	0.0010	–11785.5	–0.00027	1
53967.6355	0.0011	–11766.5	–0.00179	1
53968.5883	0.0019	–11763.5	–0.00075	1
53970.6512	0.0004	–11757	–0.00012	1
53973.6647	0.0004	–11747.5	–0.00051	1
54003.4887	0.0015	–11653.5	0.00104	1
55158.6320	0.0002	–8012.5	0.00211	2
55503.6511	0.0002	–6925	0.00138	3
56947.9765	[a]	–2372.5	0.00241	4
57679.5754	0.0002	–66.5	0.00064	5
57690.5193	0.0001	–32	–0.00091	5
57693.5339	0.0002	–22.5	–0.00028	5
57697.4986	0.0002	–10	–0.00132	5
57700.6719	0.0002	0	–0.00062	5

[a] *Not reported. References: 1. SuperWASP; 2. Diethelm (2010); 3. Diethelm (2011); 4. Nagai (2015); 5. This study at UO.*

best fit LC simulations. A hot spot on the secondary star was incorporated during Roche modeling of NSVS 7245866 (Figure 11), while a cool spot on each component was necessary to achieve the best fit of LC data for V685 Peg (Figure 12). A statistically meaningful ($l_3 > 0$) third light contribution was evident in all bandpasses during DC optimization for NSVS 7245866. Since each system clearly undergoes a total eclipse, Roche model convergence to a unique value for q is self-evident, thereby obviating the need for any "q-search" exercise. These general findings are described in more detail within the subsections for each variable that follow.

3.4. Roche modeling results

In general, it is not possible to unambiguously determine the mass ratio, subtype (A or W), or total mass without radial velocity (RV) data. Nonetheless, since a total eclipse is observed in the LCs from both systems, a unique mass ratio value for each system could be found (Terrell and Wilson 2005). Standard errors reported in Tables 6 and 7 are computed from the DC covariance matrix and only reflect the model fit to the observations which assumes exact values for any fixed parameter. These errors are generally regarded as unrealistically small, considering the estimated uncertainties associated with the mean adopted T_{eff1} values along with basic assumptions about $A_{1,2}$, $g_{1,2}$ and the influence of spots added to the Roche model. Normally, the value for T_{eff1} is fixed with no error during modeling with the WD code despite measurement uncertainty which can arguably approach 10% relative standard deviation (R.S.D.) without supporting spectral data. The effect that such uncertainty in T_{eff1} would have on modeling estimates for q, i, $\Omega_{1,2}$, and T_{eff2} has been investigated with other overcontact binaries including A- (Alton 2019) and W-subtypes (Alton and Nelson 2018). As might be expected, any change in the fixed value for T_{eff1} results in a corresponding change in the T_{eff2}. These results are notably consistent whereby the uncertainty in the model fit for T_{eff2} would be essentially the same as that established for T_{eff1}. For example, with NSVS 7245866, the expected uncertainty for T_{eff2} would be ±267 K. Furthermore, varying T_{eff1} by as much as 10% did not appreciably affect the uncertainty estimates (R.S.D. < 2%) for i, q, or $\Omega_{1,2}$ (Alton 2019; Alton and Nelson 2018). Assuming that the actual T_{eff1} values for NSVS 7245866 and V685 Peg fall within 10% of the adopted values used for Roche modeling (a reasonable presumption according to results presented in section 3.2), then uncertainty estimates for i, q, or $\Omega_{1,2}$ along with spot size, temperature, and location would likely not exceed 2% R.S.D.

The fill-out parameter (f) which corresponds to the outer surface shared by each star was calculated according to Equation 4 (Kallrath and Milone 1999; Bradstreet 2005) where:

$$f = (\Omega_{inner} - \Omega_{1,2})/(\Omega_{inner} - \Omega_{outer}), \quad (4)$$

wherein Ω_{outer} is the outer critical Roche equipotential, Ω_{inner} is the value for the inner critical Roche equipotential, and $\Omega = \Omega_{1,2}$ denotes the common envelope surface potential for the binary system. In both cases the systems are considered overcontact since $0 < f < 1$.

3.4.1. NSVS 7245866

LC parameters and geometric elements derived from WDWINT56A are summarized in Table 6. According to Binnendijk (1970) the deepest minimum (Min I) of an A-type overcontact system occurs when the cooler and less massive constituent transits across the face of the hotter and more massive star. Therefore, the flat-bottomed dip in brightness at Min II is indicative of a total eclipse of the secondary. It was evident that NSVS 7245866 is most likely an A-type overcontact binary given other diagnostic clues such as its spectral class (F5V) and orbital period (P > 0.4 d). Consequently, WD modeling proceeded under this assumption. It became immediately apparent that model-simulated LCs at Min I and Min II were consistently deeper than the observed values in all three bandpasses. This result was remediated by allowing the third light parameter (l_3) to freely vary during DC optimization. These findings (Table 6) suggest the presence of a blue-rich ($l_3(B) > l_3(V)$ or $l_3(I_c)$) field star in the distant background that has contaminated the light from NSVS 7245866. Analysis of potential secular changes in the orbital period that might arise from the influence of a third gravitational body is not possible at this time due to the limited availability of precise eclipse timing data. Despite the lack of supporting evidence for a stellar body in close

Table 4. Estimation of effective temperature (T_{eff1}) of NSVS 7245866 based upon dereddened (B–V) data from five surveys and the present study.

	USNO-B1.0	*USNO-A2.0*	*2MASS*	*APASS DR9*	*UCAC4*	*Present Study*
$(B–V)_0$[a]	0.651	0.628	0.399	0.505	0.505	0.425
T_{eff1}[b] (K)	5766	5824	6684	6260	6260	6574
Spectral Class[b]	G2V-G3V	G1V-G2V	F3V-F4V	F6V-F7V	F6V-F7V	F4V-F5V

[a] *Intrinsic $(B–V)_0$ determined using reddening value E(B–V) = 0.027 ± 0.004.*
[b] *T_{eff1} interpolated and spectral class range estimated from Pecaut and Mamajek (2013). Median value, $(B–V)_0$ = 0.505 ± 0.093, corresponds to an F6V-F7V primary star (T_{eff1} = 6260 ± 333 K).*

Table 5. Estimation of effective temperature (T_{eff1}) of V685 Peg based upon dereddened (B–V) data from five surveys and the present study.

	USNO-A2.0	*2MASS*	*SDSS-DR8*	*UCAC4*	*APASS DR9*	*Present Study*
$(B–V)_0$[a]	0.808	0.657	0.708	0.728	0.826	0.687
T_{eff1}[b] (K)	5293	5740	5562	5505	5244	5641
Spectral Class[b]	G9V-K0V	G2V-G3V	G6V-G7V	G7V-G8V	K0V-K1V	G5V-G6V

[a] *Intrinsic $(B–V)_0$ determined using reddening value E(B–V) = 0.028 ± 0.001.*
[b] *T_{eff1} interpolated and spectral class range estimated from Pecaut and Mamajek (2013). Median value, $(B–V)_0$ = 0.718 ± 0.047, corresponds to a G7V-G8V primary star (T_{eff1} = 5520 ± 186 K).*

Table 6. Light curve parameters evaluated by Roche modeling and the geometric elements derived for NSVS 7245866 assuming it is an A-type W UMa variable.

Parameter	*No spot*	*Hot spot*
T_{eff1} (K)[b]	6230 (267)	6230 (267)
T_{eff2} (K)	6366 (3)	6351 (3)
q (m_2 / m_1)	0.359 (1)	0.350 (1)
A[b]	0.5	0.5
g[b]	0.32	0.32
$\Omega_1 = \Omega_2$	2.526 (2)	2.504 (2)
i°	87.1 (3)	87.2 (3)
$A_S = T_s / T_\star$[c]	—	1.08 (1)
Θ_S (spot co-latitude)[c]	—	90 (7)
φ_S (spot longitude)[c]	—	351 (1)
r_S (angular radius)[c]	—	23 (1)
$L_1 / (L_1 + L_2)_B$[d]	0.6855 (3)	0.6925 (2)
$L_1 / (L_1 + L_2)_V$	0.6923 (1)	0.6986 (1)
$L_1 / (L_1 + L_2)_{Ic}$	0.6985 (1)	0.7040 (1)
l_3 (B)[e]	0.7372 (64)	0.8820 (56)
l_3 (V)	0.5357 (27)	0.5400 (27)
l_3 (I_c)	0.2702 (17)	0.2677 (17)
r_1 (pole)	0.4548 (3)	0.4578 (2)
r_1 (side)	0.4902 (4)	0.4941 (3)
r_1 (back)	0.5215 (5)	0.5255 (5)
r_2 (pole)	0.2886 (8)	0.2874 (2)
r_2 (side)	0.3028 (10)	0.3017 (3)
r_2 (back)	0.3474 (19)	0.3474 (5)
Fill-out factor (%)	30.6	32.6
RMS (B)[f]	0.00781	0.00755
RMS (V)	0.00561	0.00511
RMS (I_c)	0.00451	0.00432

[a] *All uncertainty estimates for T_{eff2}, q, $\Omega_{1,2}$, i, $r_{1,2}$, and L_1 from WDWINT56a (Nelson 2009).*
[b] *Fixed with no error during DC.*
[c] *Secondary star spot parameters in degrees (Θ_S, φ_S and r_S) or A_S in fractional degrees (K).*
[d] *L_1 and L_2 refer to scaled luminosities of the primary and secondary stars, respectively.* [e] *Fractional percent luminosity of third light parameter (l_3) at φ = 0.25.*
[f] *Monochromatic residual mean square error from observed values.*

Table 7. Lightcurve parameters evaluated by Roche modeling and the geometric elements derived for V685 Peg assuming it is a W-type W UMa variable.

Parameter	*No spot*	*Cool spots*
T_{eff1} (K)[b]	5521 (168)	5521 (168)
T_{eff2} (K)	5842 (5)	5774 (2)
q (m_2 / m_1)	0.386 (1)	0.404 (1)
A[b]	0.5	0.5
g[b]	0.32	0.32
$\Omega_1 = \Omega_2$	2.620 (2)	2.643 (3)
i°	89.8 (2)	87.0 (4)
$A_P = T_s / T_\star$[c]	—	0.79 (1)
Θ_P (spot co-latitude)	—	90 (1)
φ_P (spot longitude)	—	189 (1)
r_P (angular radius)	—	12.0 (1)
$A_S = T_s / T_\star$[d]	—	0.78 (1)
Θ_S (spot co-latitude)	—	90 (1)
φ_S (spot longitude)	—	103 (1)
r_S (angular radius)	—	19.9 (1)
$L_1 / (L_1 + L_2)_B$[e]	0.6260 (4)	0.6317 (2)
$L_1 / (L_1 + L_2)_V$	0.6468 (3)	0.6482 (1)
$L_1 / (L_1 + L_2)_{Ic}$	0.6627 (2)	0.6609 (1)
r_1 (pole)	0.4413 (6)	0.4398 (4)
r_1 (side)	0.4727 (7)	0.4712 (5)
r_1 (back)	0.5014 (8)	0.5011 (5)
r_2 (pole)	0.2859 (17)	0.2915 (9)
r_2 (side)	0.2988 (20)	0.3051 (11)
r_2 (back)	0.3359 (36)	0.3439 (20)
Fill-out factor (%)	12.9	17.3
RMS (B)[f]	0.01622	0.00943
RMS (V)	0.01520	0.00735
RMS (I_c)	0.01249	0.00590

[a] *All uncertainty estimates for T_{eff2}, q, $\Omega_{1,2}$, i, $r_{1,2}$, and L_1 from WDWINT56a (Nelson 2009).*
[b] *Fixed with no error during DC.*
[c] *Primary star spot parameters in degrees (Θ_P, φ_P and r_P) or A_P in fractional degrees (K).*
[d] *Secondary star spot parameters in degrees (Θ_S, φ_S and r_S) or A_S in fractional degrees (K).*
[e] *L_1 and L_2 refer to scaled luminosities of the primary and secondary stars, respectively.*
[f] *Monochromatic residual mean square error from observed values.*

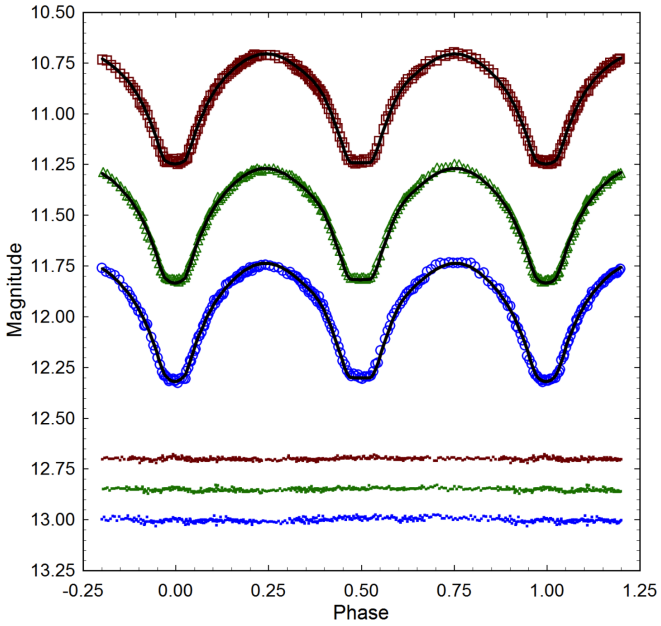

Figure 7. Folded CCD light curves for NSVS 7245866 produced from photometric data obtained between February 18, 2017, and March 6, 2017. The top (I_c), middle (V), and bottom curve (B) shown above were reduced to MPOSC3-based catalog magnitudes using MPO CANOPUS. In this case, the Roche model assumed an A-type overcontact binary with a third light contribution and no spots; residuals from the model fits are offset at the bottom of the plot to keep the values on scale.

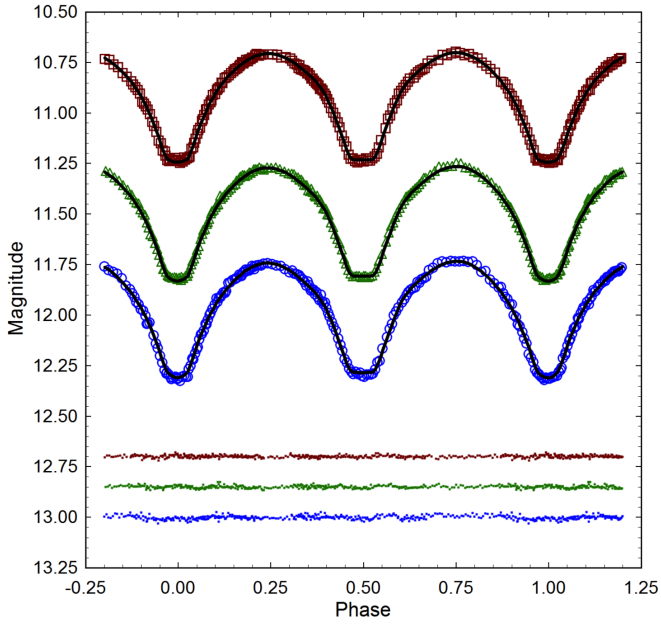

Figure 8. CCD light curves for NSVS 7245866 as shown in Figure 7 except that this case, the Roche model assumed an A-type overcontact binary with a hot spot on the secondary star.

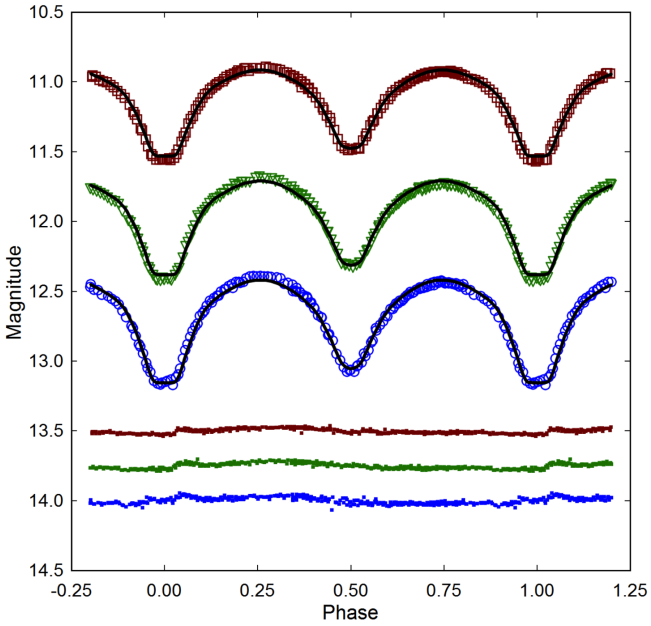

Figure 9. Folded CCD light curves for V685 Peg produced from photometric data obtained between October 18, 2016, and November 8, 2016. The top (I_c), middle (V), and bottom curve (B) shown above were reduced to MPOSC3-based catalog magnitudes using MPO CANOPUS. In this case, the Roche model assumed a W-type overcontact binary with no spots; residuals from the model fits are offset at the bottom of the plot to keep the values on scale.

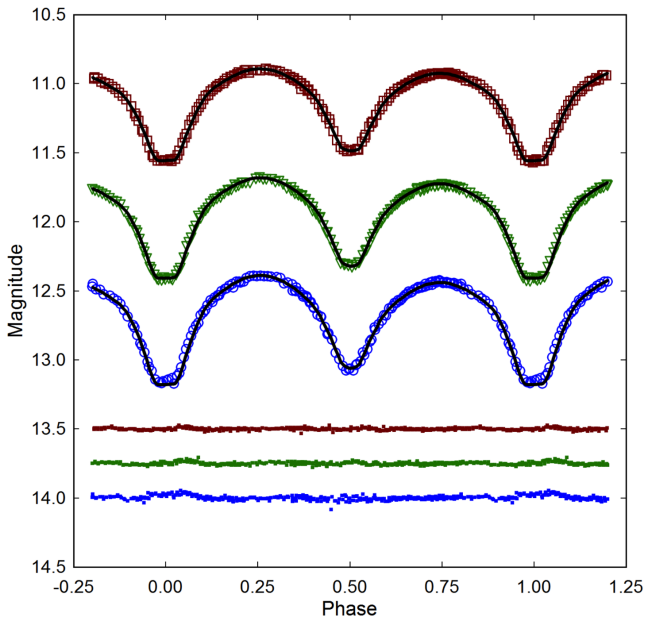

Figure 10. CCD light curves for V685 Peg as in Figure 9, however in this case, the Roche model assumed a W-type overcontact binary with a cool spot on both stars.

proximity, the presence of a hot main sequence star in the same neighborhood as NSVS 7245866 would likely overwhelm any photometric measurement, thereby discounting this possibility. However unlikely, a nearby faint blue object such as a white dwarf could satisfactorily explain the blue-rich third light.

In order to address the slight asymmetry observed during maximum light (Max I < Max II), a hot spot was added near the neck of the secondary star. This provided a modest improvement to the light curve fits during Min II (Figure 8) as reflected in the lower residual mean square error compared to that obtained from the unspotted fit (Table 6). A three-dimensional image rendered (Figure 11) using BINARY MAKER 3 (BM3; Bradstreet and Steelman 2004) illustrates the secondary star transit across the primary face during Min I ($\varphi = 0$) and the hot spot location on the secondary star ($\varphi = 0.68$). Also, it should be noted that contrary to expectations for an A-type system, the best fit of the LC data occurred when the effective temperature of the secondary star (T_{eff2}) was higher (121–136 K) than the primary

Table 8. Fundamental stellar parameters for NSVS 7245866 using the mean photometric mass ratio ($q_{ptm} = m_2/m_1$) from the spotted Roche model fits of LC data (2017) and the estimated mass based on empirically derived M-PRs for overcontact binary systems.

Parameter	*Primary*	*Secondary*
Mass ($M_\odot$)	1.38 ± 0.08	0.48 ± 0.03
Radius ($R_\odot$)	1.34 ± 0.02	0.83 ± 0.01
a ($R_\odot$)	2.84 ± 0.04	2.84 ± 0.04
Luminosity ($L_\odot$)	2.43 ± 0.42	1.01 ± 0.03
M_{bol}	3.79 ± 0.03	4.74 ± 0.03
Log (g)	4.32 ± 0.03	4.28 ± 0.03

Table 9. Fundamental stellar parameters for V685 Peg using the mean photometric mass ratio ($q_{ptm} = m_2 / m_1$) from the spotted Roche model fits of LC data (2016) and the estimated mass based on empirically derived M-PRs for W UMa type variable stars.

Parameter	*Primary*	*Secondary*
Mass ($M_\odot$)	1.17 ± 0.07	0.47 ± 0.03
Radius ($R_\odot$)	1.06 ± 0.02	0.70 ± 0.01
a ($R_\odot$)	2.31 ± 0.03	2.31 ± 0.03
Luminosity ($L_\odot$)	0.94 ± 0.12	0.49 ± 0.01
M_{bol}	4.81 ± 0.03	5.52 ± 0.03
Log (g)	4.46 ± 0.03	4.42 ± 0.03

(T_{eff1}) component (Table 6). Not without precedence, this phenomenon has also been observed for EK Com (Deb *et al.* 2010), HV Aqr (Gazeas *et al.* 2007), BO CVn (Zola *et al.* 2012), and TYC 1664-0110-1 (Alton and Stępień 2016).

3.4.2. V685 Peg

V685 Peg would appear to be a W-subtype overcontact binary system based on its spectral classification (G7V), orbital period ($P < 0.4$ d), and LC behavior. As shown in Figures 9 and 10, the flattened bottom at the deepest minimum (Min I) results from the occultation of the hotter secondary by the larger, but cooler primary star. Since according to the convention used herein where the primary star is the most massive ($m_2/m_1 \leq 1$), a phase shift (0.5) was introduced to properly align the LC for subsequent Roche modeling. LC parameters and geometric elements with their associated uncertainty were derived using WDWINT56A (Table 7). The best LC fits were obtained by the addition of a single cool spot on each star. A three-dimensional rendering produced using BM3 (Figure 12) shows a transit of the hotter secondary across the face of the primary star during Min II ($\varphi = 0.5$) and the location of each spot on the binary pair ($\varphi = 0.83$).

3.5. Absolute parameters

Fundamental stellar parameters were estimated for each binary system using results from the best fit spotted LC simulations. However, without the benefit of RV data which define the orbital motion, mass ratio, and total mass of the binary pair, these results should be more accurately described as "relative" rather than "absolute" parameters and considered preliminary in that regard.

3.5.1. NSVS 7245866

Three empirically derived mass-period relationships (M-PR) for W UMa-binaries have been published. The first M-PR was reported by Qian (2003) while two others followed from Gazeas and Stępień (2008) and then Gazeas (2009). According to Qian (2003) when the primary star is less than 1.35 $M_\odot$ or the system is W-type its mass can be determined from Equation 5:

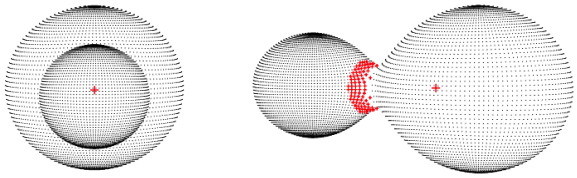

Figure 11. Three-dimensional spatial model of NSVS 7245866 illustrating the transit of the secondary star across the primary star face at Min I ($\varphi = 0$) and hot spot location ($\varphi = 0.68$) near the neck region of the secondary star.

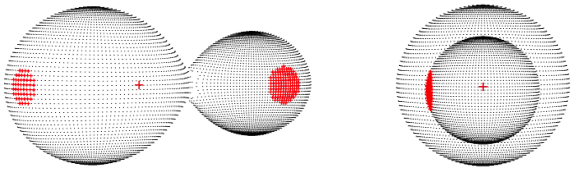

Figure 12. Three-dimensional spatial model of V685 Peg showing a transit of the hotter secondary across the face of the cooler primary star at Min II ($\varphi = 0.5$) and the locations of a single cool spot on each of the binary constituents ($\varphi = 0.83$).

$$\log(M_1) = 0.391\,(59) \cdot \log(P) + 1.96\,(17), \quad (5)$$

or alternatively when $M_1 > 1.35\ M_\odot$ or A-type then Equation 6:

$$\log(M_{-1}) = 0.761\,(150) \cdot \log(P) + 1.82\,(28), \quad (6)$$

where P is the orbital period in days. Using the most appropriate relationship (Equation 6) leads to $M_1 = 1.50 \pm 0.19\ M_\odot$ for the primary. The M-PR (Equation 7) derived by Gazeas and Stępień (2008):

$$\log(M_1) = 0.755\,(59) \cdot \log(P) + 0.416\,(24), \quad (7)$$

corresponds to a W UMa system where $M_1 = 1.32 \pm 0.10\ M_\odot$. Gazeas (2009) reported another empirical relationship (Equation 8) for the more massive (M_1) star of a contact binary such that:

$$\log(M_1) = 0.725\,(59) \cdot \log(P) - 0.076\,(32) \cdot \log(q) + 0.365\,(32), \quad (8)$$

from which $M_1 = 1.30 \pm 0.13\ M_\odot$. The mean of three values ($M_1 = 1.38 \pm 0.08\ M_\odot$) estimated from empirical models (Equations 6, 7, and 8) was used for subsequent determinations of M_2, semi-major axis a, volume-radii r_L, and bolometric magnitudes (M_{bol}) for NSVS 7245866.

The secondary mass $= 0.48 \pm 0.03\ M_\odot$ and total mass ($1.86 \pm 0.09\ M_\odot$) of the system were consequently determined using the mean photometric mass ratio (0.350 ± 0.001) from the spotted Roche model. By comparison, a single MS star with a mass similar to the secondary (late K-type) would likely be much smaller ($R_\odot \sim 0.54$), cooler ($T_{eff} \sim 3900$ K), and far less luminous ($L_\odot \sim 0.06$). The semi-major axis, $a(R_\odot) = 2.84 \pm 0.04$, was calculated from Newton's version (Equation 9) of Kepler's third law where:

$$a^3 = (G \cdot P^2 (M_1 + M_2)) / (4\pi^2). \quad (9)$$

The effective radius of each Roche lobe (r_L) can be calculated over the entire range of mass ratios ($0 < q < \infty$) according to an expression (Equation 10) derived by Eggleton (1983):

$$r_L = (0.49q^{2/3}) / (0.6q^{2/3} + \ln(1 + q^{1/3})), \quad (10)$$

from which values for r_1 (0.4917 ± 0.0002) and r_2 (0.2928 ± 0.0002) were determined for the primary and secondary stars, respectively. Since the semi-major axis and the volume radii are known, the radii in solar units for both binary components can be calculated where $R_1 = a \cdot r_1 = 1.34 \pm 0.02\, R_\odot$ and $R_2 = a \cdot r_2 = 0.83 \pm 0.01\, R_\odot$.

Luminosity in solar units ($L_\odot$) for the primary (L_1) and secondary stars (L_2) was calculated from the well-known relationship derived from the Stefan-Boltzmann law (Equation 11) where:

$$L_{1,2} = (R_{1,2} / R_\odot)^2 (T_{1,2} / T_\odot)^4. \quad (11)$$

Assuming that $T_{eff1} = 6230$ K, $T_{eff2} = 6351$ K, and $T_\odot = 5772$ K, then the solar luminosities ($L_\odot$) for the primary and secondary are $L_1 = 2.43 \pm 0.42$ and $L_2 = 1.01 \pm 0.03$, respectively. According to the Gaia DR2 release of stellar parameters (Andrae *et al.* 2018), the reported T_{eff} (6066^{+202}_{-140} K) is probably not meaningfully different from the adopted T_{eff1} (6230 ± 136 K) value. However, the predicted size ($R_\odot = 1.64^{+0.08}_{-0.10}$) and luminosity ($L_\odot = 3.30^{+0.101}_{-0.102}$) for the primary star in NSVS 7245866 are greater than the corresponding values generated by the study herein. Based on the Bailer-Jones (2015) correction for parallax data in Gaia DR2 this system can be found at a distance of $391.2^{+8.7}_{-8.4}$ pc. By comparison, using values (V_{max}, A_V, and M_V) independently derived herein, the distance modulus equation corrected for interstellar extinction places NSVS 7245866 about 13% closer (341 ± 31 pc) to the Gaia DR2 determination which is presently regarded as the "gold-standard" for Galactic distances.

3.5.2. V685 Peg

To estimate the primary star mass for V685 Peg (Table 9) the same approach described for NSVS 7245866 was used. In this case, the M-PRs (Equations 5, 7, 8) lead to a mean value of $1.17 \pm 0.07\, M_\odot$ for the primary star. The secondary mass ($0.47 \pm 0.03\, M_\odot$) and total mass ($1.65 \pm 0.07\, M_\odot$) of the system were derived from the spotted model photometric mass ratio (0.404 ± 0.001). Assuming solar-like metallicity, a solitary main sequence star with a similar mass (late K-type to early M-type) would probably be much smaller ($R_\odot \sim 0.52$), cooler ($T_{eff} \sim 3600$ K), and much less luminous ($L_\odot < 0.06$). The semi-major axis ($a(R_\odot)$), the effective radius of each Roche lobe (r_L), the radii in solar units ($R_\odot$), and the luminosities in solar units ($L_\odot$) were calculated as described for NSVS 7245866. According to the Gaia DR2 release of stellar parameters (Andrae *et al.* 2018), the reported Teff (5355^{+149}_{-92} K) is not meaningfully different from the adopted value ($T_{eff1} = 5521 \pm 168$ K) used herein. Likewise, the Gaia DR2 reported size ($R_\odot = 1.12^{+0.04}_{-0.06}$) and luminosity ($L_\odot = 0.925^{+0.018}_{-0.018}$) of the primary star are comparable to values estimated by the study herein (Table 9). According to the Bailer-Jones (2015) correction for parallax-derived distances reported in Gaia DR2 (Gaia Collab. *et al.* 2018) this system is $257.3^{+2.62}_{-2.56}$ pc away. A value independently derived from the distance modulus equation using data generated at UO places V685 Peg at a similarly distant 262 5 pc.

4. Conclusions

New times of minimum for NSVS 7245866 (n = 45) and V685 Peg (n = 32) based on multicolor CCD data (BVI_c) acquired at UO and values extrapolated from the SuperWASP survey are reported herein. These along with a few other published values led to a new linear ephemeris for each system. Eclipse timings from NSVS 7245866 also produced what appears to be a quadratic relationship suggesting that the orbital period might be increasing at a rate of $0.033\ s \cdot y^{-1}$. Both systems will require many more years of precise eclipse timing data to further substantiate any potential change(s) in orbital period. The adopted effective temperatures (T_{eff1}) for NSVS 7245866 (6230 ± 267 K) and V685 Peg (5521 ± 168 K) were based on a composite of four sources that notably included values from the Gaia DR2 release of stellar characteristics (Andrae *et al.* 2018) and estimates from LAMOST DR5 spectral data (Zhao *et al.* 2012; Wang *et al.* 2019). Both overcontact systems clearly experience a total eclipse which is evident as a flattened bottom during minimum light. Since NSVS 7245866 is most likely an A-type W UMa variable, this feature is observed during Min II. By contrast, V685 Peg exhibits a flattened bottom during its deepest minimum light (Min I) as would be expected from a W-type overcontact eclipsing binary. The photometric mass ratios for NSVS 7245866 ($q_{ptm} = 0.350$) and V685 Peg ($q_{ptm} = 0.404$) determined by Roche modeling of each totally eclipsing system should prove to be reliable substitutes for mass ratios derived from RV data. Nonetheless, spectroscopic studies (RV and high resolution classification spectra) will be required to unequivocally determine a total mass and spectral class for both systems.

5. Acknowledgements

This research has made use of the SIMBAD database operated at Centre de Données astronomiques de Strasbourg, France. In addition, the Northern Sky Variability Survey hosted by the Los Alamos National Laboratory (https://skydot.lanl.gov/nsvs/nsvs.php), the All Sky Automated Survey Catalogue of Variable Stars (http://www.astrouw.edu.pl/asas/?page=acvs), and the Catalina Surveys Data Release 2 archives maintained at http://nesssi.cacr.caltech.edu/DataRelease/ were mined for essential information. This work also presents results from the European Space Agency (ESA) space mission Gaia. Gaia data are being processed by the Gaia Data Processing and Analysis Consortium (DPAC). Funding for the DPAC is provided by national institutions, in particular the institutions participating in the Gaia MultiLateral Agreement (MLA). The Gaia mission website is https://www.cosmos.esa.int/gaia. The Gaia archive website is https://archives.esac.esa.int/gaia. This paper makes use of data from the first public release of the WASP data as

provided by the WASP consortium and services at the NASA Exoplanet Archive, which is operated by the California Institute of Technology, under contract with the National Aeronautics and Space Administration under the Exoplanet Exploration Program. The use of public data from LAMOST is also acknowledged. Guoshoujing Telescope (the Large Sky Area Multi-Object Fiber Spectroscopic Telescope LAMOST) is a National Major Scientific Project built by the Chinese Academy of Sciences. Funding for the project has been provided by the National Development and Reform Commission. LAMOST is operated and managed by the National Astronomical Observatories, Chinese Academy of Sciences.

The careful review and helpful commentary provided by Dr. Joel Eaton is gratefully acknowledged.

References

Akerlof, C., *et al.* 2000, *Astron. J.*, **119**, 1901.
Almeida, L. A., *et al.* 2015, *Astrophys. J.*, **812**, 102.
Alton, K. B. 2016, *J. Amer. Assoc. Var. Star Obs.*, **44**, 87.
Alton, K. B. 2019, *J. Amer. Assoc. Var. Star Obs.*, **47**, 7.
Alton, K. B., and Nelson, R. H. 2018, *Mon. Not. Roy. Astron. Soc.*, **479**, 3197.
Alton, K. B., and Stępień, K. 2016, Acta Astron., 66, 357.
Amôres, E. B., Moitinho, A., Arsenijevic, V., and Sodré, L 2011, in *Star Clusters in the Era of Large Surveys*, eds. A. Moitinho, J. Alves, Springer, Berlin-Heidelberg, 93.
Andrae, R., *et al.* 2018, *Astron. Astrophys.*, **616A**, 8.
Applegate, J. H. 1992, *Astrophys. J.*, **385**, 621.
Arbutina, B. 2009, *Mon. Not. Roy. Astron. Soc.*, **394**, 501.
Bailer-Jones, C. A. L. 2015, *Publ. Astron. Soc. Pacific*, **127**, 994.
Binnendijk, L. 1970, *Vistas Astron.*, **12**, 217.
Bradstreet, D. H. 2005, in *The Society for Astronomical Sciences 24th Annual Symposium on Telescope Science*, Society for Astronomical Science, Rancho Cucamonga, CA, 23.
Bradstreet, D. H., and Steelman, D. P. 2004, BINARY MAKER 3, contact software (http://www.binarymaker.com).
Butters, O. W., *et al.* 2010, *Astron. Astrophys.*, **520**, L10.
Christiansen, J. L., *et al.* 2008, *Mon. Not. R. Astron. Soc.*, **385**, 1749.
Deb, S., Singh, H. P., Seshadri, T. R., and Gupta, R. 2010, *New Astron.*, **15**, 662.
Diethelm, R. 2010, *Inf. Bull. Var. Stars*, No. 5920, 1.
Diethelm, R. 2011, *Inf. Bull. Var. Stars*, No. 5960, 1.
Drake, A. J., *et al.* 2014, *Astrophys. J., Suppl. Ser.*, **213**, 9.
Eggleton, P. P. 1983, *Astrophys. J.*, **268**, 368.
Gaia Collaboration, Brown, A.G.A., *et al.* 2018, *Astron. Astrophys.*, **616A**, 1.
Gazeas, K. D. 2009, *Commun. Asteroseismology*, **159**, 129.
Gazeas, K. D., Niarchos, P. G., and Zola, S. 2007, in *Solar and Stellar Physics Through Eclipses*, ASP Conf. Ser. 370, Astronomical Society of the Pacific, San Francisco, 279.
Gazeas, K., and Stępień, K. 2008, *Mon. Not. Roy. Astron. Soc.*, **390**, 1577.
Gettel, S. J., Geske, M. T., and McKay, T. A. 2006, *Astron. J.*, **131**, 621.
Giménez, A., Guinan, E., Niarchos, P., and Ruciński, S., eds. 2006, *Close Binaries in the 21st Century: New Opportunities and Challenges*, Springer, Dordrecht.
Houdashelt, M. L., Bell, R. A., and Sweigart, A. V. 2000, *Astron. J.*, **119**, 1448.
Kallrath, J., and Milone, E. F. 1999, *Eclipsing Binary Stars: Modeling and Analysis*, Springer, New York.
Kurucz, R. L. 2002, *Baltic Astron.*, **11**, 101.
Kwee, K. K., and van Woerden, H. 1956, *Bull. Astron. Inst. Netherlands*, **12**, 327.
Lucy, L. B. 1967, *Z. Astrophys.*, **65**, 89.
Minor Planet Observer. 2011, MPO Software Suite (http://www.minorplanetobserver.com), BDW Publishing, Colorado Springs.
Mochnacki, S. W., and Doughty, N. A. 1972, *Mon. Not. Royal Astron. Soc.*, **156**, 51.
Nagai, K. 2015, *Bull. Var. Star Obs. League Japan*, **59**, 7.
Nelson, R. H. 2009, WDWINT56A: Astronomy Software by Bob Nelson (https://www.variablestarssouth.org/bob-nelson).
O'Connell, D. J. K. 1951, *Publ. Riverview Coll. Obs.*, **2**, 85.
Paunzen, E., and Vanmunster, T. 2016, *Astron. Nachr.*, **337**, 239.
Paczyński, B., Sienkiewicz, R., and Szczygiel, D. M. 2007, *Mon. Not. Roy. Astron. Soc.*, **378**, 961.
Paczyński, B., Szczygiel, D. M., Pilecki, B. and Pojmański, G. 2006, *Mon. Not. Royal Astron. Soc.*, **368**, 1311
Pecaut, M., and Mamajek, E. E. 2013, *Astrophys. J., Suppl. Ser.*, **208**, 9.
Pojmański, G., Pilecki, B., and Szczygiel, D. 2005, *Acta Astron.*, **55**, 275.
Prša, A., and Zwitter, T. 2005, *Astrophys. J.*, **628**, 426.
Prša, A., *et al.* 2011, *Astron. J.*, **141**, 83
Qian, S-B. 2003, *Mon. Not. Roy. Astron. Soc.*, **342**, 1260.
Qian, S., Yang, Y., Zhu, L., H., He, J., and Yuan, J. 2006, *Astrophys. Space Sci.*, **304**, 25
QtiPlot. 2013, QTIPLOT v0.9.9-rc9, Data analysis and scientific visualisation (https://www.qtiplot.com/).
Ruciński, S. M. 1969, *Acta Astron.*, **19**, 245.
Wang, R., *et al.* 2019, *Pub. Astron. Soc. Pacifc*, **131**, 024505
Schwarzenberg-Czerny, A. 1996, *Astrophys. J., Lett.*, **460**, 107.
Sriram, K., Malu, S., Choi, C.S., and Vivekananda Rao, P. 2016, *Astron. J.*, **151**, 69.
Stępień, K. 2006, *Acta Astron.*, **56**, 199.
Stępień, K., and Kiraga, M. 2015, *Astron. Astrophys.*, **577A**, 117.
Terrell, D., and Wilson, R. E. 2005, *Astrophys. Space Sci.*, **296**, 221.
van Hamme, W. 1993, *Astron. J.*, **106**, 2096.
Warner, B. D. 2007, *Minor Planet Bull.*, **34**, 113.
Wilson, R. E. 1979, *Astrophys. J.*, **234**, 1054.
Wilson, R. E. 1990, *Astrophys. J.*, **356**, 613.
Wilson, R. E., and Devinney, E. J. 1971, *Astrophys. J.*, **166**, 605.
Wozniak, P. R., *et al.* 2004, *Astron. J.*, **127**, 2436.
Zhao, G., Zhao, Y.-H., Chu, Y.-Q., Jing, Y.-P, and Deng, L.-C. 2012, *Res. Astron. Astrophys.*, **12**, 723.
Zola, S., Nelson, R. H., Şenavcı, H. V., Szymanski, T., Kuźmicz, A., Winiarski, M., and Jableka, D. 2012, *New Astron.*, **17**, 673.